Age dating of an early Milky Way merger via asteroseismology of the naked-eye star ν Indi

William J. Chaplin[1,2,3], Aldo M. Serenelli[4,5,3], Andrea Miglio[1,2], Thierry Morel[6], J. Ted Mackereth[1,2], Fiorenzo Vincenzo[1,2], Hans Kjeldsen[2,7], Sarbani Basu[8], Warrick H. Ball[1,2], Amalie Stokholm[2], Kuldeep Verma[2], Jakob Rørsted Mosumgaard[2], Victor Silva Aguirre[2], Anwesh Mazumdar[9], Pritesh Ranadive[9], H. M. Antia[10], Yveline Lebreton[11,12], Joel Ong[8], Thierry Appourchaux[13], Timothy R. Bedding[14,2,3], Jørgen Christensen-Dalsgaard[2,3], Orlagh Creevey[15], Rafael A. García[16,17], Rasmus Handberg[2], D. Huber[18,3], Steven D. Kawaler[19,3], Mikkel N. Lund[2,3], Travis S. Metcalfe[20,21], Keivan G. Stassun[22,23], Michäel Bazot[24,25], Keaton J. Bell[21,2], Derek L. Buzasi[26], Othman Benomar[25,27], Diego Bossini[28], Lisa Bugnet[16,17], Tiago L. Campante[28,29], Zeynep Çelik Orhan[30], Enrico Corsaro[31], Lucıa Gonzalez Cuesta[32,33], Guy R. Davies[1,2], Maria Pia Di Mauro[34], Yvonne P. Elsworth[1,2], Patrick Gaulme[21,35], Hamed Ghasemi[36], Zhao Guo[37,38], Oliver J. Hall[1,2], Amir Hasanzadeh[36], Saskia Hekker[21,2], Rachel Howe[1,2], Jon M. Jenkins[39], Antonio Jiménez[32,33], René Kiefer[40], James S. Kuszlewicz[21,2], Thomas Kallinger[41], David W. Latham[42], Mia S. Lundkvist[2], Savita Mathur[32,33], Josefina Montalbán[1,2], Benoit Mosser[11], Martin Bo Nielsen[1,2], Sibel Örtel[30], Ben M. Rendle[1,2], George R. Ricker[43], Thaíse S. Rodrigues[44], Ian W. Roxburgh[45,1], Hossein Safari[36], Mathew Schofield[1,2], Sara Seager[43,46,47], Barry Smalley[48], Dennis Stello[49,14,2], Róbert Szabó[50,51], Jamie Tayar[18,55] Nathalie Themeßl[21,2], Alexandra E. L. Thomas[1,2], Roland K. Vanderspek[43], Walter Van Rossem[1,2], Mathieu Vrard[28,29], Achim Weiss[52] Timothy M. White[53,2], Joshua N. Winn[54], Mutlu Yıldız[29]

[1] *School of Physics and Astronomy, University of Birmingham, Birmingham B15 2TT, UK*
[2] *Stellar Astrophysics Centre (SAC), Department of Physics and Astronomy, Aarhus University, Ny Munkegade 120, DK-8000 Aarhus C, Denmark*
[3] *Kavli Institute for Theoretical Physics, University of California, Santa Barbara, CA 93106, USA*
[4] *Institute of Space Sciences (ICE, CSIC) Campus UAB, Carrer de Can Magrans s/n, 08193 Barcelona, Spain*
[5] *Institut d'Estudis Espacials de Catalunya (IEEC), C/ Gran Capità, 2-4, 08034 Barcelona, Spain*
[6] *Space sciences, Technologies and Astrophysics Research (STAR) Institute, Université de Liège, Quartier Agora, Allée du 6 Août 19c, Bât. B5C, B4000-Liège, Belgium*
[7] *Institute of Theoretical Physics and Astronomy, Vilnius University, Sauletekio av. 3, 10257 Vilnius, Lithuania*
[8] *Department of Astronomy, Yale University, P.O. Box 208101, New Haven, CT 06520-8101, USA*
[9] *Homi Bhabha Centre for Science Education, TIFR, V. N. Purav Marg, Mankhurd, Mumbai 400088, India*
[10] *Tata Institute of Fundamental Research, Mumbai, India*
[11] *LESIA, Observatoire de Paris, PSL Research University, CNRS, Sorbonne Université, Université Paris Diderot, 92195 Meudon, France*
[12] *Univ Rennes, CNRS, IPR (Institut de Physique de Rennes) - UMR 6251, F-35000 Rennes, France*
[13] *Univ. Paris-Sud, Institut d'Astrophysique Spatiale, UMR 8617, CNRS, Bâtiment 121, 91405 Orsay Cedex, France*
[14] *Sydney Institute for Astronomy (SIfA), School of Physics, University of Sydney, NSW 2006, Australia*
[15] *Université Côte d'Azur, Observatoire de la Cte d'Azur, CNRS, Laboratoire Lagrange, France*

[16] IRFU, CEA, Université Paris-Saclay, F-91191 Gif-sur-Yvette, France
[17] AIM, CEA, CNRS, Université Paris-Saclay, Université Paris Diderot, Sorbonne Paris Cité, F-91191 Gif-sur-Yvette, France
[18] Institute for Astronomy, University of Hawai'i, 2680 Woodlawn Drive, Honolulu, HI 96822, USA
[19] Department of Physics and Astronomy, Iowa State University, Ames, IA 50011
[20] Space Science Institute, 4750 Walnut Street, Suite 205, Boulder CO 80301, USA
[21] Max-Planck-Institut für Sonnensystemforschung, Justus-von-Liebig-Weg 3, 37077 Göttingen, Germany
[22] Vanderbilt University, Department of Physics & Astronomy, 6301 Stevenson Center Ln., Nashville, TN 37235, USA
[23] Vanderbilt Initiative in Data-intensive Astrophysics (VIDA), 6301 Stevenson Center Lane, Nashville, TN 37235, USA
[24] Division of Sciences, New York University Abu Dhabi, United Arab Emirates,
[25] Center for Space Science, NYUAD Institute, New York University Abu Dhabi, PO Box 129188, Abu Dhabi, United Arab Emirates
[26] Dept. of Chemistry and Physics, Florida Gulf Coast University, 10501 FGCU Blvd. S., Fort Myers, FL 33965 USA
[27] Division of Solar and Plasma Astrophysics, NAOJ, Mitaka, Tokyo, Japan
[28] Instituto de Astrofísica e Ciências do Espaço, Universidade do Porto, CAUP, Rua das Estrelas, 4150-762 Porto, Portugal
[29] Departamento de Física e Astronomia, Faculdade de Ciências da Universidade do Porto, Rua do Campo Alegre, s/n, PT4169-007 Porto, Portugal
[30] Department of Astronomy and Space Sciences, Science Faculty, Ege University, 35100, Bornova, İzmir, Turkey
[31] INAF - Osservatorio Astrofisico di Catania, via S. Sofia 78, 95123, Catania, Italy
[32] Instituto de Astrofísica de Canarias (IAC), E-38205 La Laguna,Tenerife, Spain
[33] Universidad de La Laguna (ULL), Departamento de Astrofisica, E-38206 La Laguna, Tenerife, Spain
[34] INAF-IAPS, Istituto di Astrofisica e Planetologia Spaziali, Via del Fosso del Cavaliere 100, I-00133 Roma, Italy
[35] Department of Astronomy, New Mexico State University, P.O. Box 30001, MSC 4500, Las Cruces, NM 88003-8001, USA
[36] Department of Physics, Institute for Advanced Studies in Basic Sciences (IASBS), Zanjan 45137-66731, Iran
[37] Center for Exoplanets and Habitable Worlds, 525 Davey Laboratory, The Pennsylvania State University, University Park, PA 16802, USA
[38] Department of Astronomy Astrophysics, 525 Davey Laboratory, The Pennsylvania State University, University Park, PA, 16802, USA
[39] NASA Ames Research Center, Moffett Field, CA, 94035
[40] Centre for Fusion, Space, and Astrophysics, Department of Physics, University of Warwick, Coventry, UK
[41] Institute of Astronomy, University of Vienna, 1180 Vienna, Austria
[42] Center for Astrophysics | Harvard & Smithsonian, 60 Garden Street, Cambridge, MA 02138, USA
[43] Department of Physics, and Kavli Institute for Astrophysics and Space Research, Massachusetts Institute of Technology, Cambridge, MA 02139, USA
[44] Osservatorio Astronomico di Padova – INAF, Vicolo dell'Osservatorio 5, I-35122 Padova, Italy
[45] Astronomy Unit, Queen Mary University of London, Mile End Road, London, E1 4NS, UK

[46]*Department of Earth, Atmospheric and Planetary Sciences, Massachusetts Institute of Technology, Cambridge, MA 02139, USA*
[47]*Department of Aeronautics and Astronautics, MIT, 77 Massachusetts Avenue, Cambridge, MA 02139, USA*
[48]*Astrophysics Group, Lennard-Jones Laboratories, Keele University, Staffordshire ST5 5BG, United Kingdom*
[49]*School of Physics, The University of New South Wales, Sydney NSW 2052, Australia*
[50]*Konkoly Observatory, MTA CSFK, H-1121, Konkoly Thege Miklós út 15-17, Budapest, Hungary*
[51]*MTA CSFK Lendület Near-Field Cosmology Research Group*
[52]*Max-Planck-Institut fr̈ Astrophysik, Karl-Schwarzschild-Str. 1, D-85748 Garching, Germany*
[53]*Research School of Astronomy and Astrophysics, Mount Stromlo Observatory, The Australian National University, Canberra, ACT 2611, Australia*
[54]*Department of Astrophysical Sciences, Princeton University, Princeton, NJ 08544, USA*
[55]*Hubble Fellow*

Over its 13 billion year history, the Milky Way has ingested multiple smaller satellite galaxies[1]. While these accreted stellar populations can be forensically identified as kinematically distinct structures within the Galaxy, it is difficult in general to precisely date the age at which any one merger occurred. Recent results have revealed a population of stars that were accreted via the collision of a dwarf galaxy, called *Gaia*-Enceladus[2]. This event led to a significant pollution of the chemical and dynamical properties of the Milky Way. Here, we identify the very bright, naked-eye star ν Indi as a probe of the age of the early in situ population of the Galaxy. We combine asteroseismic, spectroscopic, astrometric, and kinematic observations to show that this metal-poor, alpha-element-rich star was an indigenous member of the Milky Way, and we measure its age to be 11.0 ± 0.7 (stat) ± 0.8 (sys) Gyr. The star bears hallmarks that are consistent with it being one of the in situ population that was kinematically heated by the *Gaia*-Enceladus collision. Our age estimate would then imply that the earliest epoch at which the merger could have occurred was $\simeq 11.5$ Gyr ago at 68 % confidence and $\simeq 12.9$ Gyr ago at 95 % confidence. Moreover, the excellent constraints on age, chemistry and kinematics make ν Indi a prototype for the in situ population of stars that pre-date significant chemical enrichment of the Galaxy by Type Ia supernovae.

The recently launched NASA *Transiting Exoplanet Survey Satellite* (*TESS*)[3] has opened the brightest stars across $\simeq 80\,\%$ of the sky to micro-magnitude photometric studies in its two-year nominal mission. These are stars visible to the naked eye, which present huge opportunities for detailed characterization, study and follow-up. ν Indi (HR 8515; HD 211998; HIP 110618) is a very bright (visual apparent magnitude $V = 5.3$) metal-poor subgiant, which was observed by *TESS* during its first month of science operations. Based on nearly continuous photometric data with 2-minute time sampling, we are able to measure a rich spectrum of solar-like oscillations in the star. Combining these asteroseismic data with newly analyzed chemical abundances from ground-based spectroscopy, together with astrometry and kinematics from *Gaia*-DR2[4], show this single star is a powerful, representative tracer of old in situ stellar populations in the Galaxy. The results on ν Indi allow us to place new constraints on the epoch of the *Gaia*-Enceladus merger.

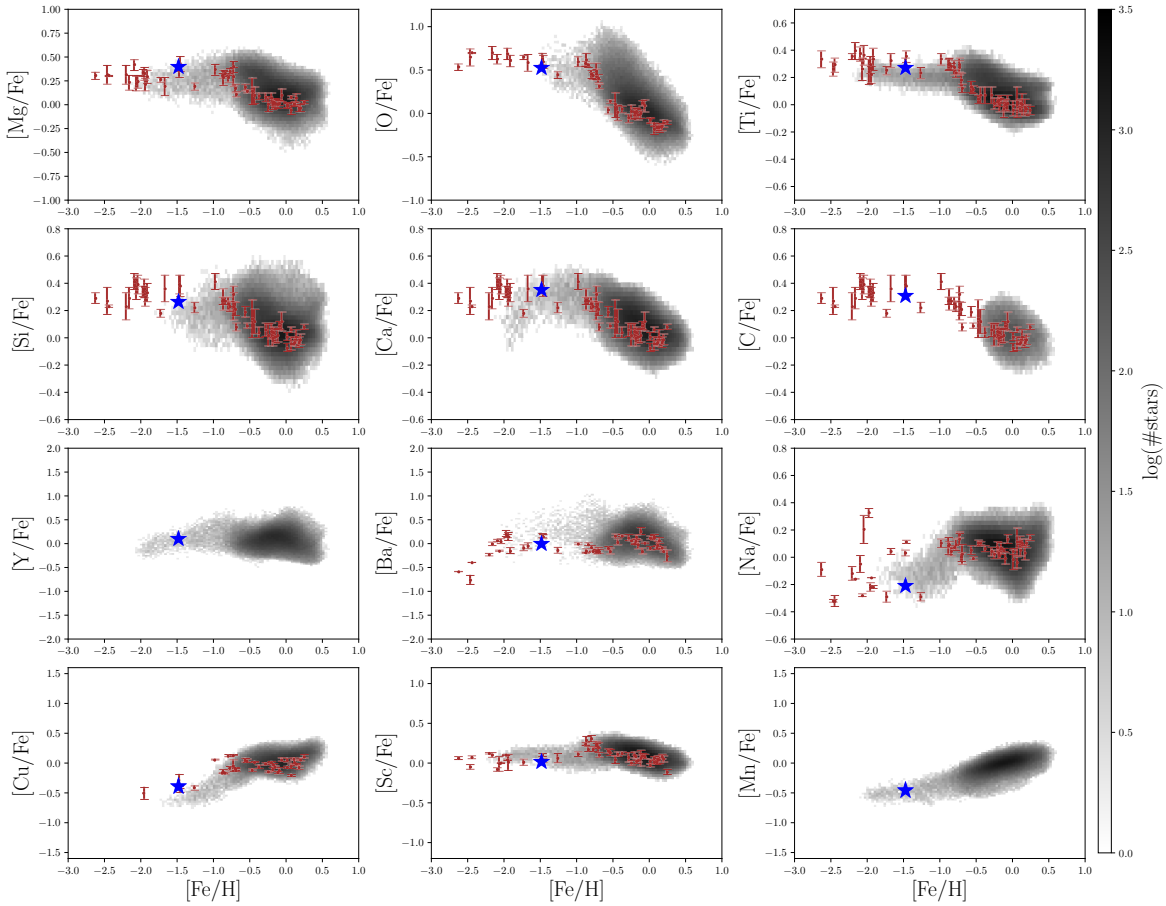

Figure 1: **Chemical abundances of ν Indi (blue star-shaped symbols) compared with those for two different samples of Milky Way stars. Shown in grey are results from the GALactic Archaeology with HERMES (GALAH) survey on stars with robust abundances from good S/N (>20) data[5]. The red points with errors show results on a sample of metal-poor F and G-type dwarfs in the local solar neighbourhood[6].**

We re-analysed archival high-resolution spectroscopic data on ν Indi collected by the *High Accuracy Radial velocity Planet Searcher* (*HARPS*) spectrograph[7] on the European Southern Observatory (ESO) 3.6-m telescope at La Silla, and by the *Fiber-fed Extended Range Optical Spectrograph* (*FEROS*)[8] on the 2.2-m ESO/MPG telescope (also at La Silla). From these high-resolution spectra we measured the overall iron abundance as well as detailed abundances for 20 different elements, providing a comprehensive set of data on the chemistry of the star (see Table 1 in **Methods**, and Fig. 1 for plots for some elements). ν Indi exhibits enhanced levels of α-process elements in its spectrum, i.e., elements heavier than carbon produced by nuclear reactions involving helium. The logarithmic abundance of α elements relative to iron is $[\alpha/\mathrm{Fe}] = +0.4\,\mathrm{dex}$ richer than in the Sun. The Galactic enhancement of α elements is believed to have happened on short timescales, through production by the core collapse of massive stars as Type II supernovae. Enhancement of iron, which occurs predominantly through the thermonuclear explosion of white dwarf stars as Type Ia supernovae, took much longer, and elevated [α/Fe] levels are therefore associated with old stellar populations. ν Indi shows an overabundance of Titanium of $[\mathrm{Ti/Fe}] = 0.27 \pm 0.07\,\mathrm{dex}$ compared to the Sun, which puts it in the regime where a previous study[9] found ages exceeding $\approx 9.5\,\mathrm{Gyr}$ for α-enhanced stars in the local solar neighbourhood, where ν Indi resides.

Recent results[10,11] using data from *Gaia*-DR2 and the *Apache Point Observatory Galaxy Evolution Experiment* (*APOGEE*) DR14 spectroscopic survey release[12] indicate that stars showing elevated [Mg/Fe] at the level exhibited by ν Indi ($0.40 \pm 0.08\,\mathrm{dex}$) are likely to be associated with the in situ Galactic population, as opposed to the accreted halo, and were kinematically heated (i.e. to larger velocities) by the *Gaia*-Enceladus accretion episode. We note also evidence from simulations[13,14] for mergers causing heating of in situ populations.

We derived orbital parameters for ν Indi using the six-dimensional information (positions and velocities) provided by *Gaia*-DR2. By reconstructing and taking samples from the covariance matrix of the astrometric parameters, we performed orbital integrations from 1000 realisations of the initial phase-space coordinates of the star. We used the python package `galpy`[15], adopting a Milky-Way-like potential (having verified that reasonable changes to the potential did not affect the conclusions drawn from our results). In order to place ν Indi in context among other stars with similar elemental abundances, we selected stars from *APOGEE*-DR14 having [Fe/H] equal (within the uncertainties) of our measured value for ν Indi (see **Methods**). We performed the same orbital integrations for populations with low and high [Mg/Fe] (which roughly divides between in situ and accreted halo stars)[10,11,16]. Fig. 2 shows a contour plot of the resulting distributions of the eccentricity, e, and maximum vertical excursion from the Galactic mid-plane, z_{max}. The low [Mg/Fe] group includes many stars in the high-eccentricity accreted halo (which was recently determined to be dominated by the *Gaia*-Enceladus accretion event). The higher [Mg/Fe] stars have lower eccentricities, and are likely part of the thick disc/in situ halo. The position of ν Indi is marked on the contour plot; the uncertainties are too small to be visible on this scale. Our analysis of the *Gaia*-DR2 data reveals that ν Indi has a relatively eccentric orbit, with $e = 0.60 \pm 0.01$, $z_{\mathrm{max}} = 1.51 \pm 0.02\,\mathrm{kpc}$, and a Galactic apocentric radius of $\simeq 2.5\,\mathrm{kpc}$. Given that ν Indi lies in a region of kinematics space which is dominated by the higher [Mg/Fe] stars, and has an [Mg/Fe]

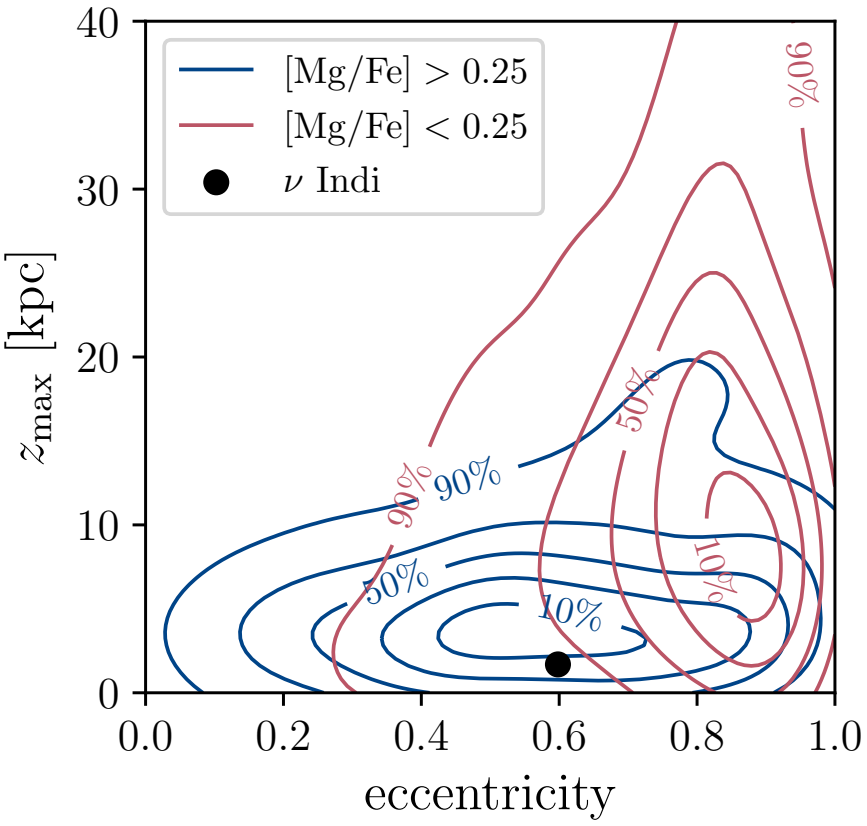

Figure 2: **Contour plot of the distribution in eccentricity, e, and maximum vertical excursion from the Galactic mid-plane, $z_{\rm max}$, of stars from *APOGEE*-DR14 having [Fe/H] lying within uncertainties of the [Fe/H] of ν Indi. The contours in blue show results for 637 stars with [Mg/Fe]>0.25, while those in red are for 918 stars with [Mg/Fe]<0.25. The solid black symbol marks the location of ν Indi. The contours are marked with the corresponding cumulative probabilities for each sample.**

abundance in-line with those stars, it is likely to be a member of this population, formed in situ (five-times more likely, based on the data in Fig. 2).

Fig. 3 shows the *Gaia*-DR2 velocity data on the two populations of stars. The cross-hair marks the location of ν Indi on both plots. The low [Mg/Fe] population shows a flat distribution (the co-called *Gaia Sausage*) in the tangential velocity versus radial velocity plane consistent with the strong radial motion expected from an accreted population. In the vertical velocity versus radial velocity plane, the distributions of the low and high [Mg/Fe] stars are remarkably similar. This is suggestive of the in-situ, higher [Mg/Fe] population, which includes ν Indi, having been heated by the accreted population.

From our discussion above we find that ν Indi is an in situ star whose age can provide insights on the origin of the low [Fe/H], high [Mg/Fe] population to which it belongs. The new asteroseis-

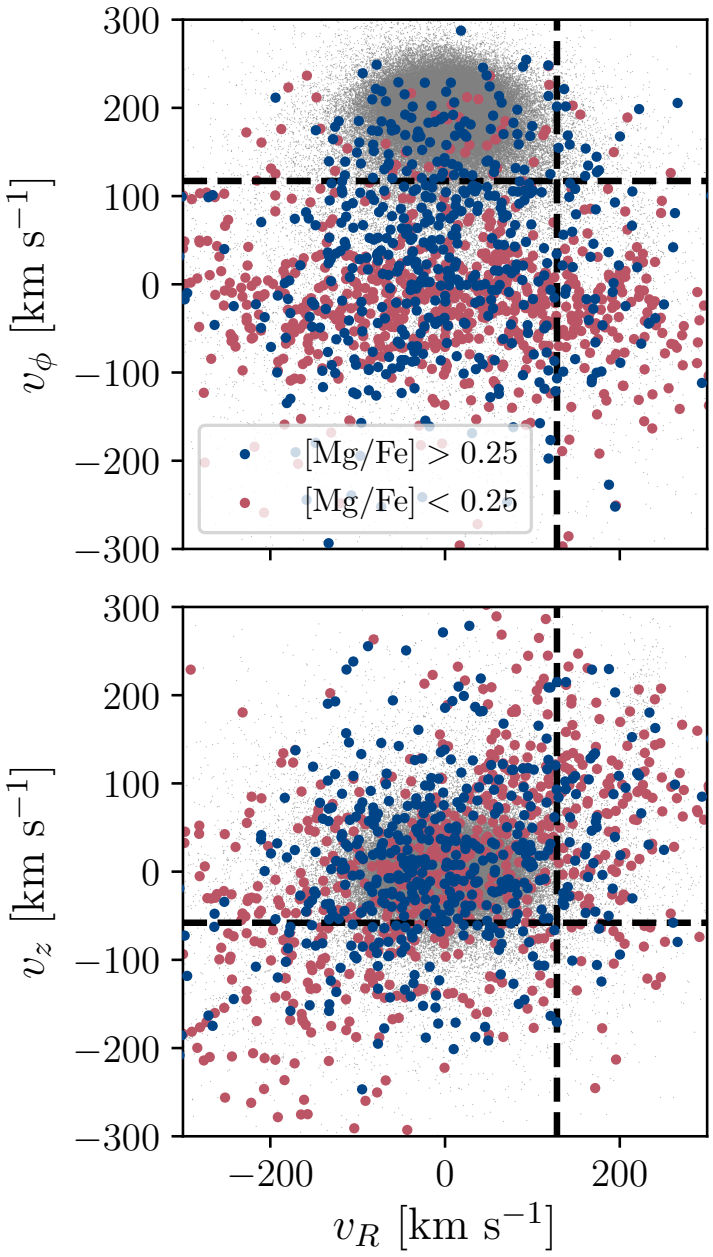

Figure 3: **Velocities for the same high (blue) and low (red) [Mg/Fe] samples as stars as Fig. 2. Plotted, in Galacto-centric cylindrical coordinates and as a function of radial velocity, are tangential velocity (upper panel) and vertical velocity (lower panel). The dashed cross-hair marks the location of ν Indi in these planes.**

mic data from *TESS* provide the means to constrain the age very precisely. ν Indi was included on the *TESS* 2-minute cadence list by the *TESS Asteroseismic Science Consortium* (*TASC*) as a prime target for asteroseismology[17]. It was observed for just over 27 days in Sector 1 of *TESS* science operations. Fig. 4 shows the frequency power spectrum of the calibrated lightcurve (see **Methods**).

The star shows a rich spectrum of overtones of solar-like oscillations, modes that are stochastically excited and intrinsically damped by near-surface convection[18]. The modes may be decomposed onto spherical harmonics of angular degree l. Overtones of radial ($l = 0$), dipole ($l = 1$) and quadrupole ($l = 2$) modes are clearly seen. Because ν Indi is an evolved star, its oscillations are most prominent in amplitude at frequencies that are significantly lower than those shown by cool, low-mass, main-sequence stars[18] like the Sun. Moreover, unlike main-sequence stars, the non-radial modes of ν Indi are not pure acoustic modes. They show so-called "mixed" character[19], due to coupling with waves confined in cavities deep within the star for which buoyancy, as opposed to gradients of pressure, act as the restoring force. The dipole modes in particular can show significant mixing. Frequencies of mixed modes change rapidly with time as the star evolves toward the red-giant phase, and are very sensitive to the structure of the deepest lying layers. They hence provide strong diagnostic constraints on the age and structure of a star.

Previous ground-based observations of precise Doppler shifts had detected solar-like oscillations in ν Indi[20], but with just a few days of data only a few oscillation modes could be identified[21]. With *TESS*, there is no ambiguity across several orders of the spectrum, and we measured frequencies of 18 modes spanning six overtones (see **Methods**). The resonant peaks in Fig. 4 are very sharp because the mode lifetimes are longer than the length of the lightcurve. As such the frequency estimates are very precise (see Table 2 in **Methods**).

To constrain the mass and age of ν Indi we used as input the measured oscillation frequencies; the spectroscopically estimated effective temperature, [Fe/H] abundance and [α/Fe] ratio; and, as another observational constraint, the stellar luminosity given by the *Gaia*-DR2 parallax and Tycho 2[22] V and B-band magnitudes. These inputs were compared, using well-developed modelling techniques[23], to intrinsic properties and predicted observables of stellar evolutionary models in evolutionary sequences sampling a dense grid in mass and composition. We find a mass of 0.85 ± 0.04 (stat) ± 0.02 (sys) $\mathrm{M}_{\odot}$ and an age of 11.0 ± 0.7 (stat) ± 0.8 (sys) Gyr. The precision achieved in mass and age is notably inferior when the asteroseismic inputs are not used (see **Methods**).

The estimated age is similar to ages from asteroseismology on a sample of old red giants[24] observed by *APOGEE* and the NASA *Kepler* Mission[25] that are believed to be thick-disc stars; and asteroseismic ages of red giants in the old globular cluster M4[26].

The asteroseismic age of ν Indi is consistent with the claim that stars in the region of [Mg/Fe]-[Fe/H] space that includes ν Indi were heated kinematically by the *Gaia*-Enceladus merger. That

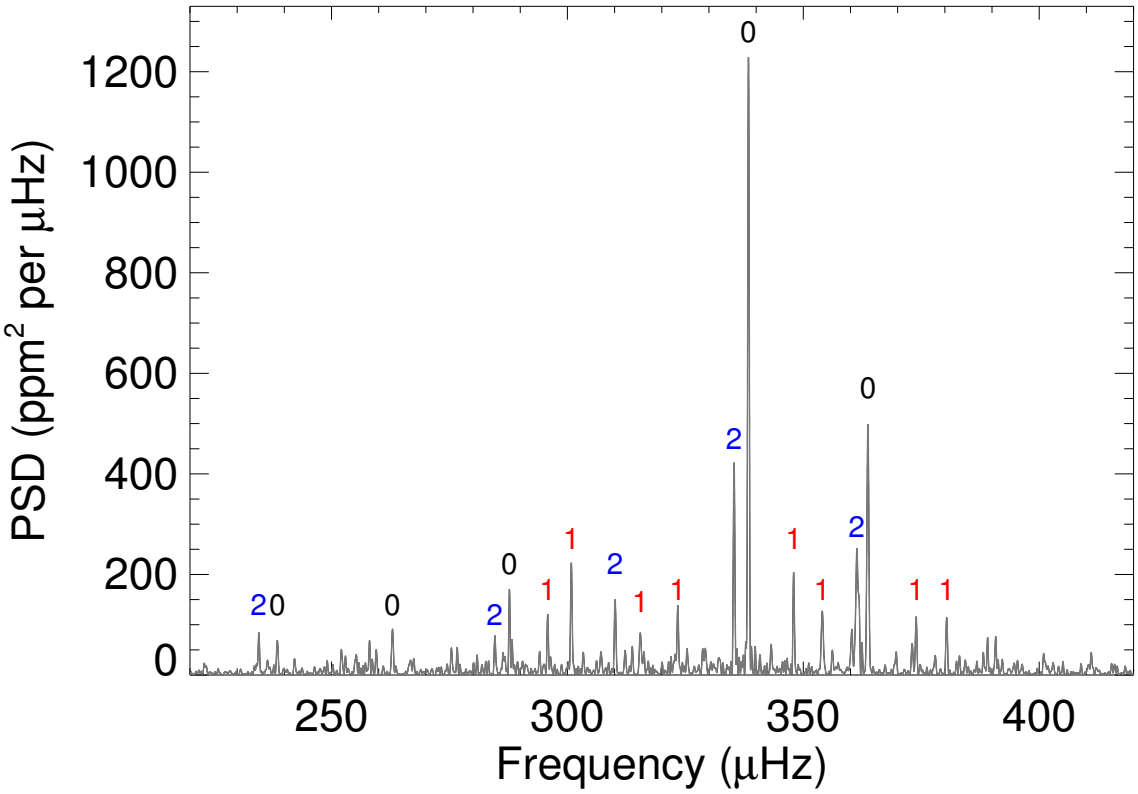

Figure 4: **Frequency-power spectrum of the *TESS* lightcurve of ν Indi, showing a rich spectrum of solar-like oscillations. Marked on the plot are the angular degrees, l, of modes whose frequencies we reported in order to model the star.**

episode has been estimated to have occurred between 9 and 12 Gyr ago [2,10,27]. Assuming it was indeed heated by the merger we may use the age of ν Indi to place a new limit on the earliest epoch at which the merger occurred (i.e., the star must have been in place to be heated by the event). We must take into account the uncertainty on our estimated age, and the potential duration in time of the merger itself. To place constraints on the latter, we estimated the dynamical friction timescale for the orbit of *Gaia*-Enceladus to decay due to the drag force exerted on it by the diffuse dark matter halo of the Milky Way. We adopted a widely-used formulation[28] and assumed that at the epoch of the merger the mass ratio between *Gaia*-Enceladus and our Galaxy was one-quarter[2], and that the orbit of *Gaia*-Enceladus was strongly radialised[29]. With these assumptions, we derive a merger timescale of less than 1 Gyr. Using our posterior on the age of ν Indi, and allowing for a spread of up to 1 Gyr for the merger (here, assuming a Gaussian profile), we estimate the earliest the merger could have occured was $11.5\,\mathrm{Gyr}$ ago at 68 % confidence, and 12.9 Gyr ago at 95 % confidence. The results are fairly insensitive to the merger duration (e.g., reducing the duration to 0.1 Gyr reduces the 95 % limit by only 0.2 Gyr).

Methods

Spectroscopic analysis

We base our chemical abundance analysis primarily on the average of six *HARPS* spectra obtained in 2007 December, retrieved from the instrument archives. They have a resolving power, R, of 115 000 and cover the spectral domain from 379 to 691 nm (with a gap between 530.4 and 533.8 nm). The signal-to-noise ratio, S/N, at 550 nm lies in the range 177 to 281. We carried out a differential, line-by-line analysis relative to the Sun. The high-quality (S/N$\sim$470) solar *HARPS* spectrum was taken from the online library of *Gaia* FGK benchmarks[30]. It is a solar reflected spectrum from asteroids with a similar resolution to that of the spectra for ν Indi. For oxygen we made use of the OI triplet at $\sim$777.4 nm. Because this range is not covered by the *HARPS* spectra, we used the spectrum available in the *FEROS* archives ($R \sim 47\,000$ and a mean S/N of 340). For the Sun, numerous asteroid spectra were considered. All the spectra were normalised to the continuum by fitting low-order cubic spline or Legendre polynomials to the line-free regions using standard tasks implemented in the *IRAF* software[31].

The stellar parameters and abundances of 20 elements were determined self-consistently from the spectra, plane-parallel *MARCS* model atmospheres[32], and the 2017 version of the line-analysis software *MOOG*. We used a line list[33] augmented[34,35] for C I, Sc II, Mn I, Co I, Cu I, Zn I, Y II, and Zr II. Equivalent widths (EW) were measured manually assuming Gaussian profiles. Only lines above 480.0 nm were considered because of strong line crowding in the blue that leads to an uncertain placement of the continuum. With the exception of Mg I λ571.1, lines with relative width RW = log(EW/λ) $>$ –4.8 were discarded. Hyperfine structure (HFS) and isotopic splitting were taken into account for Sc, V, Mn, Co, and Cu using atomic data from the Kurucz database with an assumed Cu isotopic ratio[36]. The `blends` driver in *MOOG* was employed for the analysis. The corrections are very small for ν Indi, but can be significant for the Sun. The determination of the Li and O abundances from Li I λ670.8 and [O I] λ630.0 relied on a spectral synthesis[37], taking the

macroturbulent and projected rotational velocities of ν Indi into account[38].

The four model parameters — effective temperature $T_{\rm eff}$, surface gravity $\log g$, metallicity [Fe/H] and microturbulence parameter ξ — were modified iteratively until the excitation and ionization balance of iron was fulfilled and the Fe I abundances exhibited no trend with RW. The abundances of iron and the α elements were also required to be consistent with the values adopted for the model atmosphere. For the solar analysis, $T_{\rm eff}$ and $\log\ g$ were held fixed at 5777 K and 4.44 dex, respectively, whereas the microturbulence, ξ, was left as a free parameter (we obtained $\xi_{\odot}$ = 0.97 km s^{-1}). We also performed the analysis with the surface gravity of ν Indi fixed to the asteroseismic value of $\log g = 3.46$ dex in order to increase both the accuracy and precision of the spectroscopic results. For this constrained analysis, we adjusted $T_{\rm eff}$ to satisfy iron ionization equilibrium. For both analyses (i.e., with and without the asteroseismic constraint) we corrected the iron abundances for departures from local thermodynamic equilibrium (LTE). For a representative sample of 42 Fe I features, we obtained a mean non-LTE correction[39] of ~ 0.016 dex based on the calculations. The corrections are small (less than 0.05 dex) irrespective of the line lower excitation potential or strength. Previous studies[39,40] also show, as is well known, that the Fe II lines are formed under non-LTE conditions. The line-to-line scatter of the differential Fe abundances lies in the range 0.03 to 0.06 dex. The uncertainties in the stellar parameters and abundances were computed following well-established procedures[41]. In particular, the analysis was repeated using Kurucz atmosphere models and the differences incorporated in the error budget. However, the deviations with respect to the default values (Kurucz minus MARCS) appear to be small: $\Delta T_{\rm eff}$ = –15 K, $\Delta \log g$ = –0.01 dex, and abundance ratios deviating by less than 0.01 dex.

Our analysis yielded an estimated effective temperature of $T_{\rm eff} = 5320 \pm 24$ K from the asteroseismically constrained analysis and $T_{\rm eff} = 5275 \pm 45$ K from the unconstrained analysis; and a metallicity of [Fe/H]$= -1.48 \pm 0.06$ from the constrained analysis, and [Fe/H]$= -1.51 \pm 0.07$ from the unconstrained analysis.

Detailed chemical abundances are listed in Table 1. The values in brackets give the number of features each abundance is based on. For iron, the number of Fe I and Fe II lines is given. The final iron abundance is the unweighted average of the Fe I and Fe II values. For oxygen, we adopt the value given by [O I] λ 630 because it is largely insensitive to non-LTE and 3D effects.

Asteroseismic analysis

The *TESS* target pixel file data for ν Indi were produced by the *TESS* Science Operations Center (SPOC)[42], and are available at the Mikulski Archive for Space Telescopes (MAST). The lightcurve we analysed was extracted from target pixel files by the *TESS Asteroseismic Science Operations Centre* (*TASOC*) pipeline[43]. A rich spectrum of overtones of radial- and non-radial solar-like oscillations is clearly detectable (Fig. 4). Even though the modes are intrinsically damped, the lifetimes are longer than the 27-day length of the *TESS* data. The modes may as such be treated as being coherent on the timescale of the lightcurve, and we extracted their frequencies using a well-tested weighted sine-wave fitting analysis[44,45], which allowed for the varying quality of the *TESS* pho-

tometry over the period of observation. Approaches based on fitting Lorentzian-like models to the resonant peaks[46–56] gave very similar results. Corrections to the frequencies to allow for the line-of-sight velocity of the star[57] are very small, and do not change the inferred stellar properties. The list of frequencies, together with their equivalent 1 σ uncertainties, is presented in Table 2.

The oscillation frequencies were used as input to the stellar modelling, along with spectroscopically derived effective temperature $T_{\rm eff}$, metallicity [Fe/H], and α-enhancement, [α/Fe], all from the asteroseismically constrained analysis, and an estimate of the stellar luminosity $L = 6.00 \pm 0.35\,{\rm L}_\odot$, using the *Gaia*-DR2 parallax and Tycho 2[22] V and B-band magnitudes, and a bolometric correction appropriate to the α-enhanced composition[58] (and assuming negligible extinction). We note that a Spectral Energy Distribution (SED) fit[59] gave similar constraints on luminosity.

Prior to use in the modelling we inflated the uncertainties on $T_{\rm eff}$ and [Fe/H] to account for systematic differences between spectroscopic methods by adding, respectively, 59 K and 0.062 dex in quadrature to the formal uncertainties[60], yielding final values of $T_{\rm eff} = 5320 \pm 64\,{\rm K}$ and [Fe/H]$= -1.48 \pm 0.09$.

ν Indi is a metal-poor star showing significant α enhancement, which affects the mapping of [Fe/H] to the metal-to-hydrogen abundance ratio Z/X. Some modellers used grids of stellar evolutionary models that did not include the requisite enrichment, and under such circumstances a correction must be applied to the raw [Fe/H] to allow it to be used in modelling using those grids. Here, the correction needed[61] is $+0.25\,{\rm dex}$. This gave a corrected metallicity of [Fe/H]$= -1.23 \pm 0.11$, where the error bar was inflated further to account for uncertainty in the correction.

Various codes[23,62–68] were used to model the star and to explore its fundamental stellar properties. ν Indi is in a rapid stage of stellar evolution, and we found it was imperative that the codes interrogated model grids sampled at a fine resolution in mass and metallicity in order to obtain a good match of predicted observables of the best-fitting model to the actual observables. Our best-fitting estimates are 0.85 ± 0.04 (stat) ± 0.02 (sys) ${\rm M}_\odot$ and an age of 11.0 ± 0.7 (stat) ± 0.8 (sys) ${\rm Gyr}$. The central values and statistical uncertainties were provided by one of the codes[23], which returned the best match to the input data. The systematic uncertainties reflect the scatter between different results. In all cases, the errors correspond to a 68 % confidence level.

Fig. 5 is an échelle diagram showing the good match between the observed frequencies (in grey) and the best-fitting model frequencies (coloured symbols).

We also tested the impact of removing the asteroseismic frequencies from the modelling. This inflated the fractional uncertainty on the mass (stat) from $\simeq 5\,\%$ to $\simeq 8\,\%$, and the fractional uncertainty on age from less than 10 % to more than 30 %.

1. Nissen, P. E. & Schuster, W. J. Two distinct halo populations in the solar neighborhood. Evidence from stellar abundance ratios and kinematics. *Astronomy & Astrophysics* **511**, L10 (2010). 1002.4514.

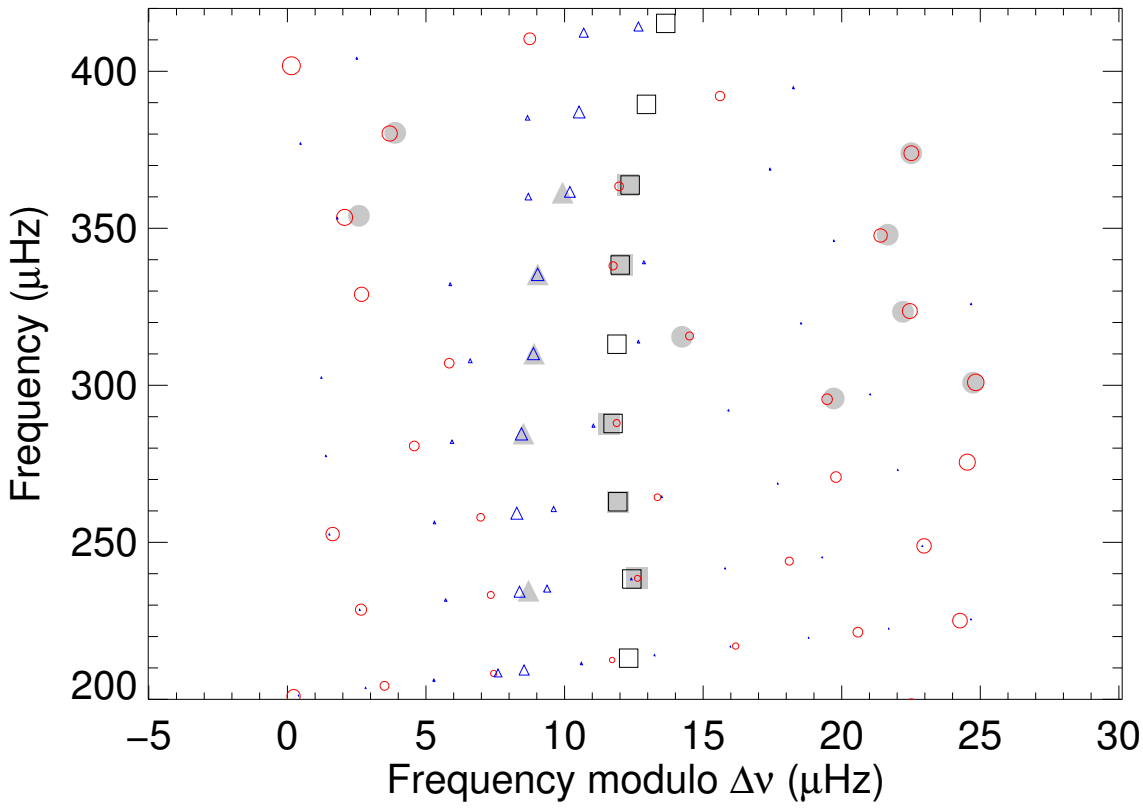

Figure 5: **An échelle diagram showing the observed frequencies (in grey) and the best-fitting model frequencies (coloured symbols). The diagram was made by dividing the spectrum into segments of length equal to the average frequency separation $\Delta\nu$ between consecutive overtones, which were then stacked in ascending order, so one plots ν versus (ν mod $\Delta\nu$). The $l = 0$ (radial) modes are plotted with square symbols, the $l = 1$ (dipole) modes with circular symbols, and the $l = 2$ (quadrupole) modes with triangular symbols. The $l = 0$ (radial) modes are plotted with square symbols, the $l = 1$ (dipole) modes with circular symbols, and the $l = 2$ (quadrupole) modes with triangular symbols. Symbol sizes reflect the relative visibilities of the different modes, with a suitable correction included to reflect the impact of mixing on the mode inertia. All model frequencies are plotted, irrespective of whether we were able to report a good observed frequency for them.**

2. Helmi, A. *et al.* The merger that led to the formation of the Milky Way's inner stellar halo and thick disk. *Nature* **563**, 85–88 (2018). 1806.06038.

3. Ricker, G. R. *et al.* Transiting Exoplanet Survey Satellite (TESS). In *Space Telescopes and Instrumentation 2014: Optical, Infrared, and Millimeter Wave*, vol. 9143 of *SPIE Proceedings*, 914320 (2014). 1406.0151.

4. Gaia Collaboration *et al.* Gaia Data Release 2. Summary of the contents and survey properties. *Astronomy & Astrophysics* **616**, A1 (2018). 1804.09365.

5. Buder, S. *et al.* The GALAH Survey: second data release. *Monthly Notices of the Royal Astronomical Society* **478**, 4513–4552 (2018). 1804.06041.

6. Zhao, G. *et al.* Systematic Non-LTE Study of the -.6 $\leq$ [Fe/H] $\leq$ 0.2 F and G Dwarfs in the Solar Neighborhood. II. Abundance Patterns from Li to Eu. *Astrophysical Journal* **833**, 225 (2016). 1610.00193.

7. Mayor, M. *et al.* Setting New Standards with HARPS. *The Messenger* **114**, 20–24 (2003).

8. Kaufer, A. *et al.* Commissioning FEROS, the new high-resolution spectrograph at La-Silla. *The Messenger* **95**, 8–12 (1999).

9. Bensby, T., Feltzing, S. & Oey, M. S. Exploring the Milky Way stellar disk. A detailed elemental abundance study of 714 F and G dwarf stars in the solar neighbourhood. *Astronomy & Astrophysics* **562**, A71 (2014). 1309.2631.

10. Di Matteo, P. *et al.* The Milky Way has no in-situ halo but it has a thick disc. Composition of the stellar halo and age-dating the last significant merger with Gaia DR2 and APOGEE. *arXiv e-prints* (2018). 1812.08232.

11. Mackereth, J. T. *et al.* The origin of accreted stellar halo populations in the Milky Way using APOGEE, Gaia, and the EAGLE simulations. *Monthly Notices of the Royal Astronomical Society* **482**, 3426–3442 (2019). 1808.00968.

12. Majewski, S. R. *et al.* The Apache Point Observatory Galactic Evolution Experiment (APOGEE). *Astronomical Journal* **154**, 94 (2017). 1509.05420.

13. Font, A. S. *et al.* Cosmological simulations of the formation of the stellar haloes around disc galaxies. **416**, 2802–2820 (2011). 1102.2526.

14. McCarthy, I. G. *et al.* Global structure and kinematics of stellar haloes in cosmological hydrodynamic simulations. **420**, 2245–2262 (2012). 1111.1747.

15. Bovy, J. galpy: A python Library for Galactic Dynamics. **216**, 29 (2015). 1412.3451.

16. Hayes, C. R. *et al.* Disentangling the Galactic Halo with APOGEE. I. Chemical and Kinematical Investigation of Distinct Metal-poor Populations. *Astrophysical Journal* **852**, 49 (2018). 1711.05781.

17. Schofield, M. *et al.* The Asteroseismic Target List (ATL) for solar-like oscillators observed in 2-minute cadence with the Transiting Exoplanet Survey Satellite (TESS). *arXiv e-prints* (2019). 1901.10148.

18. Chaplin, W. J. & Miglio, A. Asteroseismology of Solar-Type and Red-Giant Stars. *"Annual Review of Astronomy & Astrophysics"* **51**, 353–392 (2013). 1303.1957.

19. Bedding, T. R. *et al.* Gravity modes as a way to distinguish between hydrogen- and helium-burning red giant stars. **471**, 608–611 (2011). 1103.5805.

20. Bedding, T. R. *et al.* Solar-like Oscillations in the Metal-poor Subgiant ν Indi: Constraining the Mass and Age Using Asteroseismology. *Astrophysical Journal* **647**, 558–563 (2006). astro-ph/0604453.

21. Carrier, F. *et al.* Solar-like oscillations in the metal-poor subgiant ν Indi. II. Acoustic spectrum and mode lifetime. *Astronomy & Astrophysics* **470**, 1059–1063 (2007). 0706.0795.

22. Høg, E. *et al.* The Tycho-2 catalogue of the 2.5 million brightest stars. *Astronomy & Astrophysics* **355**, L27–L30 (2000).

23. Serenelli, A. *et al.* The First APOKASC Catalog of Kepler Dwarf and Subgiant Stars. **233**, 23 (2017). 1710.06858.

24. Silva Aguirre, V. *et al.* Confirming chemical clocks: asteroseismic age dissection of the Milky Way disc(s). *Monthly Notices of the Royal Astronomical Society* **475**, 5487–5500 (2018). 1710.09847.

25. Borucki, W. J. *et al.* Kepler Planet-Detection Mission: Introduction and First Results. *Science* **327**, 977 (2010).

26. Miglio, A. *et al.* Detection of solar-like oscillations in relics of the Milky Way: asteroseismology of K giants in M4 using data from the NASA K2 mission. *Monthly Notices of the Royal Astronomical Society* **461**, 760–765 (2016). 1606.02115.

27. Vincenzo, F. *et al.* The Fall of a Giant. Chemical evolution of Enceladus, alias the Gaia Sausage. *arXiv e-prints* (2019). 1903.03465.

28. Lacey, C. & Cole, S. Merger rates in hierarchical models of galaxy formation. **262**, 627–649 (1993).

29. Belokurov, V., Erkal, D., Evans, N. W., Koposov, S. E. & Deason, A. J. Co-formation of the disc and the stellar halo. **478**, 611–619 (2018). 1802.03414.

30. Blanco-Cuaresma, S., Soubiran, C., Jofré, P. & Heiter, U. The Gaia FGK benchmark stars. High resolution spectral library. *Astronomy & Astrophysics* **566**, A98 (2014). 1403.3090.

31. Tody, D. The IRAF Data Reduction and Analysis System. In Crawford, D. L. (ed.) *Instrumentation in astronomy VI*, vol. 627 of , 733 (1986).

32. Gustafsson, B. *et al.* A grid of MARCS model atmospheres for late-type stars. I. Methods and general properties. *Astronomy & Astrophysics* **486**, 951–970 (2008). 0805.0554.

33. Chen, Y. Q., Nissen, P. E., Zhao, G., Zhang, H. W. & Benoni, T. Chemical composition of 90 F and G disk dwarfs. **141**, 491–506 (2000). astro-ph/9912342.

34. Meléndez, J. *et al.* 18 Sco: A Solar Twin Rich in Refractory and Neutron-capture Elements. Implications for Chemical Tagging. *Astrophysical Journal* **791**, 14 (2014). 1406.5244.

35. Reddy, B. E., Tomkin, J., Lambert, D. L. & Allende Prieto, C. The chemical compositions of Galactic disc F and G dwarfs. *Monthly Notices of the Royal Astronomical Society* **340**, 304–340 (2003). astro-ph/0211551.

36. Asplund, M., Grevesse, N., Sauval, A. J. & Scott, P. The Chemical Composition of the Sun. *"Annual Review of Astronomy & Astrophysics"* **47**, 481–522 (2009). 0909.0948.

37. Morel, T. *et al.* Atmospheric parameters and chemical properties of red giants in the CoRoT asteroseismology fields. *Astronomy & Astrophysics* **564**, A119 (2014). 1403.4373.

38. Bruntt, H. *et al.* Accurate fundamental parameters for 23 bright solar-type stars. *Monthly Notices of the Royal Astronomical Society* **405**, 1907–1923 (2010). 1002.4268.

39. Bergemann, M., Lind, K., Collet, R., Magic, Z. & Asplund, M. Non-LTE line formation of Fe in late-type stars - I. Standard stars with 1D and 3D model atmospheres. *Monthly Notices of the Royal Astronomical Society* **427**, 27–49 (2012). 1207.2455.

40. Lind, K., Bergemann, M. & Asplund, M. Non-LTE line formation of Fe in late-type stars - II. 1D spectroscopic stellar parameters. *Monthly Notices of the Royal Astronomical Society* **427**, 50–60 (2012). 1207.2454.

41. Morel, T. The chemical composition of α Centauri AB revisited. *Astronomy & Astrophysics* **615**, A172 (2018). 1805.00929.

42. Jenkins, J. M. *et al.* The TESS science processing operations center. In *Software and Cyberinfrastructure for Astronomy IV*, vol. 9913 of , 99133E (2016).

43. Lund, M. N., Handberg, R., Kjeldsen, H., Chaplin, W. J. & Christensen-Dalsgaard, J. Data preparation for asteroseismology with TESS. In *European Physical Journal Web of Conferences*, vol. 160 of *European Physical Journal Web of Conferences*, 01005 (2017). 1610.02702.

44. Kjeldsen, H. *et al.* Solar-like Oscillations in α Centauri B. *Astrophysical Journal* **635**, 1281–1290 (2005). arXiv:astro-ph/0508609.

45. Bedding, T. R. *et al.* Solar-like Oscillations in the G2 Subgiant β Hydri from Dual-Site Observations. *Astrophysical Journal* **663**, 1315–1324 (2007). arXiv:astro-ph/0703747.

46. Benomar, O., Appourchaux, T. & Baudin, F. The solar-like oscillations of HD 49933: a Bayesian approach. **506**, 15–32 (2009).

47. Gaulme, P., Appourchaux, T. & Boumier, P. Mode width fitting with a simple Bayesian approach. Application to CoRoT targets HD 181420 and HD 49933. **506**, 7–14 (2009). 1011.2675.

48. Mosser, B. *et al.* Spin down of the core rotation in red giants. **548**, A10 (2012). 1209.3336.

49. Corsaro, E. & De Ridder, J. DIAMONDS: A new Bayesian nested sampling tool. Application to peak bagging of solar-like oscillations. **571**, A71 (2014). 1408.2515.

50. Corsaro, E., De Ridder, J. & García, R. A. Bayesian peak bagging analysis of 19 low-mass low-luminosity red giants observed with Kepler. **579**, A83 (2015). 1503.08821.

51. Vrard, M. *et al.* Helium signature in red giant oscillation patterns observed by Kepler. **579**, A84 (2015). 1505.07280.

52. Nielsen, M. B., Schunker, H., Gizon, L., Schou, J. & Ball, W. H. Limits on radial differential rotation in Sun-like stars from parametric fits to oscillation power spectra. **603**, A6 (2017). 1705.10517.

53. Roxburgh, I. W. Anomalies in the Kepler Asteroseismic Legacy Project Data A re-analysis of 16 Cyg A B, KIC 8379927 and 6 solar-like stars. **604**, A42 (2017). 1706.04408.

54. García Saravia Ortiz de Montellano, A., Hekker, S. & Themeßl, N. Automated asteroseismic peak detections. **476**, 1470–1496 (2018). 1801.09432.

55. Benomar, O. *et al.* Asteroseismic detection of latitudinal differential rotation in 13 Sun-like stars. *Science* **361**, 1231–1234 (2018). 1809.07938.

56. Kallinger, T., Beck, P. G., Stello, D. & Garcia, R. A. Non-linear seismic scaling relations. **616**, A104 (2018). 1805.06249.

57. Davies, G. R. *et al.* Why should we correct reported pulsation frequencies for stellar line-of-sight Doppler velocity shifts? **445**, L94–L98 (2014). 1408.7042.

58. Casagrande, L. & VandenBerg, D. A. Synthetic Stellar Photometry - II. Testing the bolometric flux scale and tables of bolometric corrections for the Hipparcos/Tycho, Pan-STARRS1, SkyMapper, and JWST systems. *Monthly Notices of the Royal Astronomical Society* **475**, 5023–5040 (2018). 1801.05508.

59. Stassun, K. G. & Torres, G. Eclipsing Binaries as Benchmarks for Trigonometric Parallaxes in the Gaia Era. *Astronomical Journal* **152**, 180 (2016). 1609.02579.

60. Torres, G. *et al.* Improved Spectroscopic Parameters for Transiting Planet Hosts. *Astrophysical Journal* **757**, 161 (2012). 1208.1268.

61. Salaris, M., Chieffi, A. & Straniero, O. The alpha-enhanced isochrones and their impact on the FITS to the Galactic globular cluster system. *Astrophysical Journal* **414**, 580–600 (1993).

62. Rendle, B. M. *et al.* AIMS - a new tool for stellar parameter determinations using asteroseismic constraints. *Monthly Notices of the Royal Astronomical Society* **484**, 771–786 (2019). 1901.02663.

63. Ong, J. M. J. & Basu, S. Explaining Deviations from the Scaling Relationship of the Large Frequency Separation. *Astrophysical Journal* **870**, 41 (2019). 1811.06996.

64. Silva Aguirre, V. *et al.* Standing on the Shoulders of Dwarfs: the Kepler Asteroseismic LEGACY Sample. II.Radii, Masses, and Ages. *Astrophysical Journal* **835**, 173 (2017). 1611.08776.

65. Mosumgaard, J. R., Ball, W. H., Silva Aguirre, V., Weiss, A. & Christensen-Dalsgaard, J. Stellar models with calibrated convection and temperature stratification from 3D hydrodynamics simulations. *Monthly Notices of the Royal Astronomical Society* **478**, 5650–5659 (2018). 1806.00020.

66. Ball, W. H. & Gizon, L. Surface-effect corrections for oscillation frequencies of evolved stars. *Astronomy & Astrophysics* **600**, A128 (2017). 1702.02570.

67. Lebreton, Y. & Goupil, M. J. Asteroseismology for "à la carte" stellar age-dating and weighing. Age and mass of the CoRoT exoplanet host HD 52265. *Astronomy & Astrophysics* **569**, A21 (2014). 1406.0652.

68. Yıldız, M., Çelik Orhan, Z. & Kayhan, C. Fundamental properties of Kepler and CoRoT targets - III. Tuning scaling relations using the first adiabatic exponent. *Monthly Notices of the Royal Astronomical Society* **462**, 1577–1590 (2016). 1607.03768.

Acknowledgements This paper includes data collected by the TESS mission, which are publicly available from the Mikulski Archive for Space Telescopes (MAST). Resources supporting this work were provided by the NASA High-End Computing (HEC) Program through the NASA Advanced Supercomputing (NAS) Division at Ames Research Center for the production of the SPOC data products. W.J.C. acknowledges support from the UK Science and Technology Facilities Council (STFC) and UK Space Agency. Funding for the Stellar Astrophysics Centre is provided by The Danish National Research Foundation (Grant agreement no.: DNRF106). This research was supported in part by the National Science Foundation under Grant No. NSF PHY-1748958. A.M., J.T.M., F.V., and J.M. acknowledge support from the ERC Consolidator Grant funding scheme (project ASTEROCHRONOMETRY, G.A. n. 772293). W.H.B. and M.B.N. acknowledge support from the UK Space Agency. A.M.S. is partially supported by the Spanish Government (ESP2017-82674-R) and Generalitat de Catalunya (2017-SGR-1131). T.M. acknowledges financial support from Belspo for contract PRODEX PLATO. H.K. acknowledges support from the European Social Fund via the Lithuanian Science Council grant No. 09.3.3-LMT-K-712-01-0103. S.B. acknowledges support from NSF grant AST-1514676 and NASA grant 80NSSC19K0374. V.S.A. acknowledges support

from the Independent Research Fund Denmark (Research grant 7027-00096B). T.S.M. acknowledges support from a visiting fellowship at the Max Planck Institute for Solar System Research. Computational resources were provided through XSEDE allocation TG-AST090107. D.L.B. acknowledges support from NASA under grant NNX16AB76G. T.L.C. acknowledges support from the European Union's Horizon 2020 research and innovation programme under the Marie Skłodowska-Curie grant agreement No. 792848 (PULSATION). This work was supported by FCT/MCTES through national funds (PIDDAC) by means of grant UID/FIS/04434/2019. K.J.B., S.H., J.S.K. and N.T. are supported by the European Research Council under the European Community's Seventh Framework Programme (FP7/2007-2013)/ERC grant agreement no 338251 (StellarAges). E.C. is funded by the European Union's Horizon 2020 research and innovation program under the Marie Sklodowska-Curie grant agreement No. 664931. L.G.C. acknowledges support from the MINECO FPI-SO doctoral research project SEV-2015-0548-17-2 and predoctoral contract BES-2017-082610. P.G. is supported by the German space agency (Deutsches Zentrum für Luft- und Raumfahrt) under PLATO data grant 50OO1501. R.K. acknowledges support from the UK Science and Technology Facilities Council (STFC), under consolidated grant ST/L000733/1. M.S.L. is supported by the Carlsberg Foundation (Grant agreement no.: CF17-076)". Z.C.O., S.O. and M.Y. acknowledge support from the Scientific and Technological Research Council of Turkey (TÜBİTAK:118F352). S.M. acknowledges support from the Spanish ministry through the Ramon y Cajal fellowship number RYC-2015-17697. T.S.R. acknowledges financial support from Premiale 2015 MITiC (PI B. Garilli). R. Sz. acknowledges the support from NKFIH grant project No. K-115709, and the Lendület program of the Hungarian Academy of Science, project No. 2018-7/2018. J.T. acknowledges support was provided by NASA through the NASA Hubble Fellowship grant No. 51424 awarded by the Space Telescope Science Institute, which is operated by the Association of Universities for Research in Astronomy, Inc., for NASA, under contract NAS5-26555.

Author contributions W.J.C. led the project, with help from A.M.S., A.M., S.B. and W.H.B. T.M. performed the spectroscopic analysis of the archival *HARPS* and *FEROS* data on ν Indi. H.K. led the extraction of the mode frequencies from the *TESS* lightcurve. H.K., W.J.C., T.R.B., R.A.G., D.H., K.J.B., D.L.B., O.B., T.L.C., E.C., L.G.C., G.R.D., Y.P.E., P.G., H.G., O.J.H., A.H., S.H., R.H., A.J., R.K., J.S.K., T.K., M.S.L., S.M., B.M., M.B.N., I.W.R., H.S., N.T., A.E.L.T., M.V. and T.M.W. aworked on extracting mode parameters from the *TESS* data. A.M.S., A.M., S.B., W.H.B., A.S., J.R.M., A.M., P.R., H.M.A., Y.L., J.O., J.T.M., M.B., K.J.B., Z.C.O., Z.G., S.H., J.M., S.O., B.M.R., V.S.A., D.S., J.T., W.V.R., K.V., A.W. and M.Y. worked on modelling ν Indi. J. T. M. and F. V. performed the kinematics analysis and comparison of the chemistry of ν Indi with samples of Milky Way stars. R.H. and M.N.L. oversaw production of the *TESS* lightcurves for the asteroseismic analysis. D.H., K.M.S. and B.S. provided estimates of the luminosity of ν Indi. J.C.-D., H.K., W.J.C., T.R.B., S.D.K., S.B. are key architects of TASC (members of its board), whilst G.R.R., J.M.J., D.W.L., R.K.V. J.N.W. are key architects of the TESS Mission. W.J.C., D.H., T.A., A.M.S., O.C., R.A.G. and T.S.M. oversaw the TASC working groups on solar-like oscillators, and with M.S. and T.L.C., oversaw the selection of short-cadence targets for asteroseismic studies of solar-like oscillators with *TESS*, which included ensuring ν Indi was included on the list (and hence received the *TESS* short-cadence data needed to make this study possible). W.J.C. also wrote the paper, with contributions from T.M., A.M.S., A.M., S.B., J.T.M., and F.V. All authors have contributed to the interpretation of the data and the results.

Competing Interests The authors declare that they have no competing financial interests.

Correspondence Correspondence and requests for materials should be addressed to W.J.C.. (email: w.j.chaplin@bham.ac.uk).

Table 1: Spectroscopically derived abundances

Element	Unconstrained abundance (dex)	Constrained abundance (dex)
[Fe/H]	–1.51±0.07 (58,5)	–1.48±0.06 (58,5)
[Li/H]	–0.01±0.09 (1)	+0.04±0.07 (1)
[C/Fe]	+0.33±0.09 (1)	+0.31±0.08 (1)
[O/Fe] (O I)	+0.73±0.10 (2)	+0.69±0.09 (2)
[O/Fe] ([O I])	+0.49±0.09 (1)	+0.53±0.08 (1)
[Na/Fe]	–0.20±0.10 (2)	–0.21±0.10 (2)
[Mg/Fe]	+0.42±0.08 (1)	+0.40±0.08 (1)
[Si/Fe]	+0.27±0.06 (7)	+0.26±0.06 (7)
[Ca/Fe]	+0.36±0.07 (6)	+0.35±0.06 (6)
[Sc/Fe]	+0.00±0.06 (2)	+0.02±0.06 (2)
[Ti/Fe]	+0.27±0.07 (4)	+0.27±0.07 (4)
[V/Fe]	+0.00±0.12 (3)	+0.02±0.11 (3)
[Cr/Fe]	–0.08±0.08 (1)	–0.09±0.08 (1)
[Mn/Fe]	–0.46±0.08 (3)	–0.46±0.07 (3)
[Co/Fe]	+0.18±0.10 (3)	+0.19±0.09 (3)
[Ni/Fe]	–0.08±0.07 (13)	–0.08±0.07 (13)
[Cu/Fe]	–0.38±0.08 (1)	–0.39±0.08 (1)
[Zn/Fe]	+0.16±0.09 (1)	+0.15±0.09 (1)
[Y/Fe]	+0.08±0.07 (3)	+0.10±0.07 (3)
[Zr/Fe]	+0.38±0.08 (1)	+0.40±0.08 (1)
[Ba/Fe]	–0.02±0.13 (2)	+0.00±0.13 (2)

Table 2: Measured oscillation frequencies of ν Indi

Degree, l	Frequency (μHz)	Uncertainty (μHz)
2	234.60	0.18
0	238.52	0.20
0	262.93	0.18
2	284.62	0.18
0	287.72	0.13
1	295.81	0.14
1	300.84	0.11
2	310.10	0.13
1	315.44	0.19
1	323.41	0.15
2	335.33	0.07
0	338.38	0.05
1	347.96	0.11
1	353.98	0.15
2	361.33	0.11
0	363.70	0.07
1	373.91	0.15
1	380.39	0.17